

# Mutant carbonic anhydrase 4 impairs pH regulation and causes retinal photoreceptor degeneration

Zhenglin Yang<sup>1,2,†</sup>, Bernardo V. Alvarez<sup>5,†</sup>, Christina Chakarova<sup>6,†</sup>, Li Jiang<sup>1,2</sup>, Goutam Karan<sup>1,2</sup>, Jeanne M. Frederick<sup>1</sup>, Yu Zhao<sup>1,2</sup>, Yves Sauvé<sup>1</sup>, Xi Li<sup>1,2</sup>, Eberhart Zrenner<sup>7</sup>, Bernd Wissinger<sup>7</sup>, Anneke I. Den Hollander<sup>8</sup>, Bradley Katz<sup>1</sup>, Wolfgang Baehr<sup>1,3,4</sup>, Frans P. Cremers<sup>8</sup>, Joseph R. Casey<sup>5</sup>, Shomi S. Bhattacharya<sup>6</sup> and Kang Zhang<sup>1,2,4,\*</sup>

<sup>1</sup>Department of Ophthalmology and Visual Science, University of Utah Health Science Center, Salt Lake City, UT 84112, USA, <sup>2</sup>Program in Human Molecular Biology and Genetics, Eccles Institute of Human Genetics and <sup>3</sup>Department of Biology and <sup>4</sup>Department of Neurobiology and Anatomy, University of Utah, Salt Lake City, UT 84112, USA, <sup>5</sup>CIHR Group in Molecular Biology of Membrane Proteins, Department of Physiology, University of Alberta, Edmonton, Canada T6G 2H7 and <sup>6</sup>Department of Molecular Genetics, Institute of Ophthalmology, University College London, 11-43 Bath Street, London EC1V 9EV, UK, <sup>7</sup>Universitätsaugenklinik Tübingen, Abt. Pathophysiologie des Sehens und Neuroophthalmologie, Tübingen, Germany and <sup>8</sup>Department of Human Genetics, University Medical Centre Nijmegen, PO Box 9101, 6500 HB Nijmegen, The Netherlands

Received September 16, 2004; Revised October 19, 2004; Accepted November 10, 2004

**Retina and retinal pigment epithelium (RPE) belong to the metabolically most active tissues in the human body. Efficient removal of acid load from retina and RPE is a critical function mediated by the choriocapillaris. However, the mechanism by which pH homeostasis is maintained is largely unknown. Here, we show that a functional complex of carbonic anhydrase 4 (CA4) and Na<sup>+</sup>/bicarbonate co-transporter 1 (NBC1) is specifically expressed in the choriocapillaris and that missense mutations in CA4 linked to autosomal dominant rod–cone dystrophy disrupt NBC1-mediated HCO<sub>3</sub><sup>-</sup> transport. Our results identify a novel pathogenic pathway in which a defect in a functional complex involved in maintaining pH balances, but not expressed in retina or RPE, leads to photoreceptor degeneration. The importance of a functional CA4 for survival of photoreceptors implies that CA inhibitors, which are widely used as medications, particularly in the treatment of glaucoma, may have long-term adverse effects on vision.**

## INTRODUCTION

Retinitis pigmentosa (RP) is the most prevalent group of inherited retinal degeneration, affecting approximately 1 in 3500 persons or a total of 1.8 million people worldwide (1,2). Clinical features of RP include night blindness, constriction and progressive loss of peripheral visual field affecting rod photoreceptors, followed by eventual loss of central vision (cones). RP may be transmitted as an autosomal dominant, recessive or X-linked trait (3,4). All known RP genes are expressed either in photoreceptors or in retinal pigment epithelium (RPE), and are, to the most part, involved in photoreceptor structure, phototransduction, photoreceptor development, the retinoid cycle or RNA splicing.

Retinal phototransduction is modulated by pH changes in its surrounding environment (5). It has been demonstrated that the amplitude of rod photoreceptor responses will decrease by ~70% when the extracellular pH was decreased to 6.0 (6). Furthermore, there will also be a concomitant decrease in the Na<sup>+</sup> conductance of rod photoreceptor outer segments (7). Despite exquisite sensitivity to the extracellular pH changes, photoreceptors paradoxically have a high rate of metabolism (8) and consequently high rate of endogenous acid production. As by-products of energy production in photoreceptors, a large amount of carbon dioxide and bicarbonate is generated from oxidative phosphorylation in mitochondria in the inner segments and lactic acid is generated from the inner and outer segments (9). Additional acid is

\*To whom correspondence should be addressed. Tel: +1 8015856797; Fax: +1 8015853501; Email: kzhang@hmbg.utah.edu

<sup>†</sup>The authors wish it to be known that, in their opinion, the first three authors should be regarded as joint First Authors.

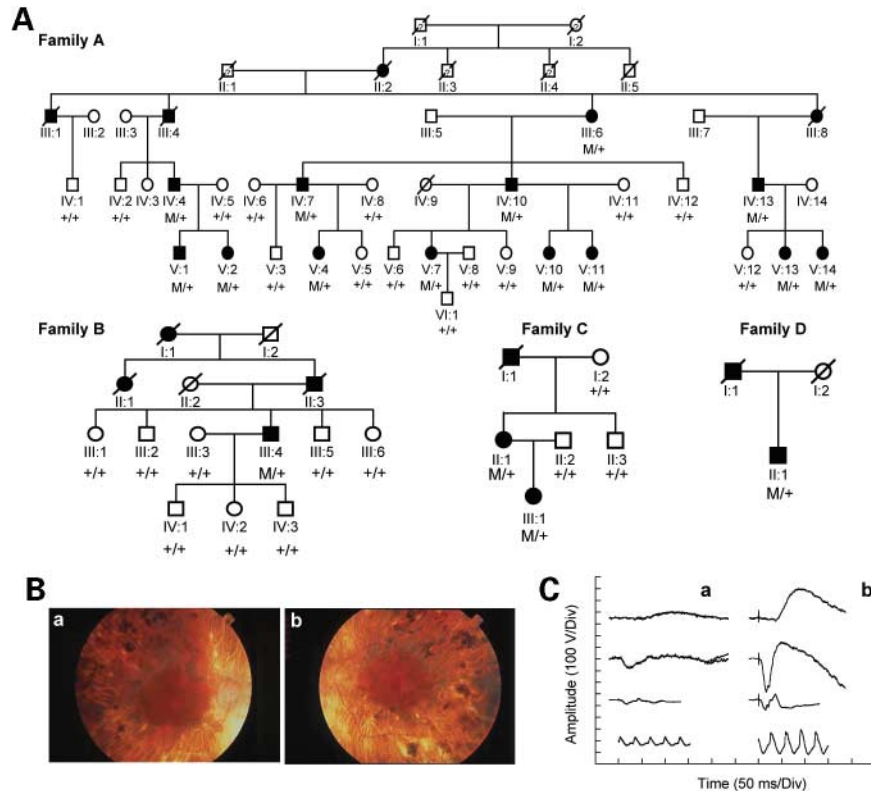


**Figure 1.** Pedigrees and clinical features of RP17. (A) Kindred structure and segregation of *CA4* mutations in family A (R14W), family B (R219S) and families C and D (G>A at +59 of 3'-UTR). Affected individuals are identified by solid squares (males) or solid circles (females). Normal individuals are identified by open symbols; deceased individuals are indicated by a slash (/). M, mutant allele of the *CA4*; +, normal allele of the *CA4*. (B) Fundus photography (a, right eye, b, left) of patient IV:13 (age 58, visual acuity light perception in both eyes) demonstrating typical bone spicule pigmentation and extensive retina and RPE atrophy. (C) ERGs recorded from patient V:14 (a) in the early course of disease compared with a normal control subject (b). The different rows indicate the different stimulus conditions: (top row: dark-adapted ERG recorded to  $-2.0 \log \text{cd s/m}^2$  stimulus; second row: dark-adapted ERG recorded to  $0.5 \log \text{cd s/m}^2$  stimulus; third row: light-adapted ERG recorded to  $0.5 \log \text{cd s/m}^2$  stimulus; fourth row: 31 Hz flicker ERG recorded to  $0.5 \log \text{cd s/m}^2$  stimulus. Successive responses from the two eyes are superimposed. Note that the ERGs of both dark-adapted eye (rod) and light-adapted eye (cone) are markedly reduced.

generated from  $\text{H}^+$  release from cGMP turnover in the outer segment (10), and  $\text{H}^+$  influx due to  $\text{Ca}^{++}/\text{H}^+$  exchanger activity in the plasma membrane of inner segment (11). The increase in acid load and lowering of intracellular pH are prevented by its removal from retina and RPE and release to blood stream in the choriocapillaris in the choroid, which is located adjacent to RPE and photoreceptors.

The electrogenic sodium bicarbonate co-transporter 1 (NBC1) mediates  $\text{Na}^+$ -coupled  $\text{HCO}_3^-$  transport across plasma membranes in many mammalian tissues including kidney, lung and heart (12,13). Originally, identified from human kidney, NBC1 was the first mammalian NBC gene cloned, and plays an essential role in  $\text{HCO}_3^-$  reabsorption in basolateral membranes of the proximal tubule of kidney, where it works in conjunction with luminal  $\text{H}^+$  transporters to secrete acid (14). Two splice variants of *NBC1* have been identified which differ in their N-terminal sequence (15). Carbonic anhydrases (CAs), a family of 14 isozymes with a wide tissue expression pattern, catalyze the reversible reaction:  $\text{CO}_2 + \text{H}_2\text{O} \rightleftharpoons \text{HCO}_3^- + \text{H}^+$ . CAs are functionally coupled with NBCs to form a complex that produces  $\text{HCO}_3^-$  for transport across membrane and that consumes  $\text{HCO}_3^-$  being transported across membranes. This functional protein complex is called the bicarbonate transport

metabolon. A metabolon is a physical complex of enzymes in a linked enzymatic pathway (16).

Recently, an R14W mutation in *CA4* was suggested to be responsible for an autosomal dominant form of RP (RP17) in a South African family (17). It was proposed that impaired *CA4*-R14W secretion, intracellular unfolded response and apoptotic cell death are responsible for photoreceptor degeneration. We performed genetic studies in several RP17 families with rod-cone dystrophy and identified several mutations in the *CA4* gene. We show that impaired pH homeostasis, rather than defective secretion of mutant *CA4*, is the most likely cause underlying the RP17 phenotype. Our results identify a novel pathogenic pathway in which a defect in a functional complex involved in maintaining pH balances, but not expressed in retina or RPE, leads to photoreceptor degeneration.

## RESULTS

### Identification of the disease gene for RP17

We conducted genetic analysis on a large Caucasian family (Fig. 1A, family A) with a rod-cone dystrophy (Fig. 1B and C). Genotype analysis demonstrated linkage to the RP17

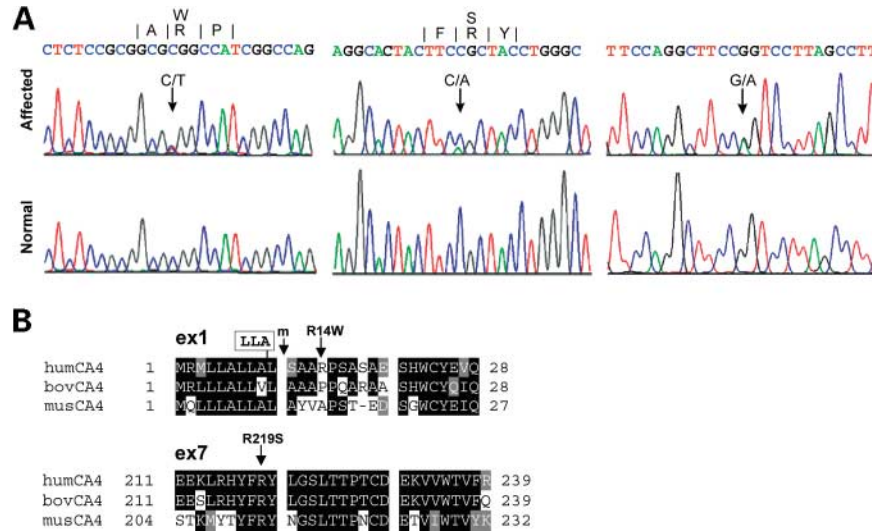


**Figure 2.** Mutations in *CA4* linked to RP17. **(A)** Automated sequencing traces revealing mutations in patients affected by RP17. Mutation detection, performed by direct sequencing of PCR products, reveals a C>T transition in exon 1 of *CA4* in family A (left panel), C>A transversion in exon 7 in family B (middle panel) and G>A transversion in 3'-UTR in families C and D (right panel) (arrows). **(B)** Partial sequence of the human *CA4* polypeptide compared with bovine and mouse orthologs. Top panel, the N-terminal region. 'm' depicts the predicted mature N-terminal; ex1 represents exon 1; LLA marks a leader sequence polymorphism (triplication of LLA motif) observed in the human population. Bottom, portion of exon 7 (ex7) containing the R219S mutation.

locus, and genealogical records indicate that it is an offshoot of the South African family described earlier (18). A two-point peak LOD score of 5.9 was obtained at  $\theta = 0.00$  with marker D17S1290. We limited the minimal genetic interval to 2.18 cM between D17S1606 and D17S948. This interval contains about 51 predicted genes (Supplementary Material, Table S1). Each exon of all genes within the interval was amplified and sequenced. A C>T transition at position 40 changing Arg<sup>14</sup> to Trp (R14W) in *CA4* (*CA4*-R14W) (Fig. 2A) was the only change in the interval that was consistent with pathology. First, it altered a positively charged amino acid presumably located in the N-terminal domain of the mature *CA4* polypeptide (Fig. 2B) which is secreted and tethered extracellularly to the cell membrane via a glycosyl-phosphatidyl inositol (GPI) anchor. Secondly, it completely segregated with the disease phenotype in the study family. We then screened 178 families with adRP (Supplementary Material, Table S2) for alterations in *CA4*. In an unrelated European family with adRP (Fig. 1A, family B), we identified a second alteration in exon 7, a C>A transversion changing Arg<sup>219</sup> to Ser (R219S). R219 is well conserved in *CA4* polypeptides among different species (Fig. 2B), and biochemical analysis shows that *CA4*-R219S is enzymatically inactive (discussed subsequently) strongly suggesting that this alteration may be pathogenic. A third alteration located outside the coding sequence (a G>A transition at +59 of the 3'-UTR) in two other unrelated adRP families (Fig. 1A, families C and D) may affect *CA4*-expression levels (discussed subsequently). None of these mutations was found in over 1000 normal control chromosomes, strongly supporting pathogenicity.

### Mutant *CA4* impairs pH regulation by NBC1

Retina and RPE belong to the metabolically most active tissues in the human body with a production of acid and

CO<sub>2</sub> even higher than in the brain (8). Efficient removal of acid load is achieved by a high rate of blood flow in choriocapillaris and the functional interaction of *CA4* and NBC1 (19). *CA4* was shown to be present in endothelial cells of the choriocapillaris (20). We showed that both components co-localize in the endothelium of the choriocapillaris in the plasma membranes (Fig. 3). The *CA4*/NBC1 metabolon is not detectable in photoreceptors or RPE. The tethering of *CA4* close to the NBC1 HCO<sub>3</sub><sup>-</sup> transport site in the plasma membrane maximizes the transmembrane HCO<sub>3</sub><sup>-</sup> gradient of this complex and thereby increases the NBC1-mediated HCO<sub>3</sub><sup>-</sup> transport rate (19).

We investigated the effect of the *CA4* mutations on the NBC1-mediated HCO<sub>3</sub><sup>-</sup> transport in HEK293 cells co-transfected with *NBC1* and *CA4* mutant cDNAs. The cells were loaded with 2', 7'-bis(2-carboxyethyl)-5(6)-carboxyfluorescein-acetoxymethyl ester (BCECF-AM) fluorescent dye to monitor intracellular pH (pH<sub>i</sub>). The bicarbonate flux associated with these cells was determined from the relation: Flux =  $\Delta\text{pH}_i/\text{time} \times \beta_{\text{total}}$ , where  $\beta_{\text{total}}$  is the total cellular H<sup>+</sup> buffering capacity that was measured for these cells (21). Figure 4A shows robust amiloride-insensitive pH<sub>i</sub> recovery following acid load, attributable to the NBC1-*CA4* interaction. Confirming previous findings, the transport rate for HEK293 cells co-transfected with *NBC1* and *CA4* cDNA was significantly higher when compared with cells expressing only NBC1 (Fig. 4A). Co-expression of wild-type NBC1 and mutant *CA4* proteins (either *CA4*-R14W or *CA4*-R219S) failed to increase the rates of intracellular pH recovery after acid load (Fig. 4A and B). Co-expression of NBC1 and a mixture of wild-type and mutant *CA4* (mimicking normal and mutant alleles in human RP17 patients) suppressed pH recovery displaying an intermediate phenotype. We found that recombinant *CA4*-R219S has no CA activity (Table 1), consistent with the location of R219 at the active cleft

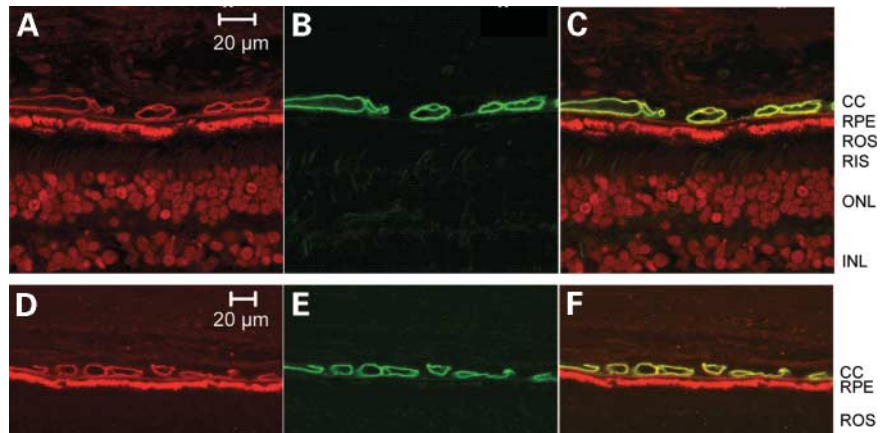


**Figure 3.** Confocal immunolocalization of CA4 and NBC1 in the human choriocapillaris. (A) Propidium iodide (red) binding defines the choriocapillaris (CC), RPE and retina layers (ONL, outer nuclear layer; INL, inner nuclear layer). (B) Anti-CA4 antibody detected by FITC (green)-conjugated secondary antibody labels endothelial cells of the choriocapillaris intensely and specifically. Immunoreactivity is associated with membranes of endothelial cells. (C) Merged image from A and B. Note that endothelia associated with larger vessels of the choroidal stroma are negative for immunoreactivity. (D) Anti-NBC1 antibody visualized with rhodamine Red<sup>TM</sup>-X-conjugated secondary antibody also labels endothelium of the choriocapillaris. Control incubations omitting the primary antibody demonstrated that fluorescence associated with the RPE is non-specific. (E) Immunolabeling of choriocapillaris endothelium by anti-CA4 antibody. (F) Merged image showing co-labeling (yellow) of identical endothelial cells in human choriocapillaris by antibodies directed against NBC1 (D) and CA4 (E). Magnification bars (A and D) = 20  $\mu$ m.

of CA4 and distortion of the catalytic center (22). The 3'-UTR + 59 mutation co-segregating with RP17 in affected patients of families C and D decreased CA4 mRNA levels in the affected patients by 30% when compared with the normal control (Supplementary Material, Fig. S1). The effect of this reduction on the levels of expressed protein has not been determined, but consistent with haplo-insufficiency, it is conceivable that reduction of functional CA4 may have a negative effect on pH regulation in the retina. A DNA sequence polymorphism, *CA4* 21\_29ins9, found in the normal control population resulted in triplication of the sequence LLA in the signal sequence of CA4 (CA4-ins L<sub>7</sub>L<sub>8</sub>A<sub>9</sub>). When co-expressed with NBC1, CA4-ins L<sub>7</sub>L<sub>8</sub>A<sub>9</sub> activated NBC1 transport activity to the same extent as wild-type CA4 did (Fig. 4B). Thus, insertion of LLA into the signal sequence did not alter CA4 activity, consistent with a benign polymorphism.

#### Defective Interaction of mutant CA4-R14W with NBC1

Gel overlay and co-immunoprecipitation assays have previously shown that NBC1 and CA4 form a complex (19). One explanation for the failure of CA4 mutants to activate NBC1 transport activity is loss of physical interaction with NBC1, perhaps caused by CA4 misfolding, or loss of CA activity. To test this hypothesis, lysates of untransfected (Fig. 4C, lane 1) and NBC1-transfected (Fig. 4C, lane 2) cells were prepared, subjected to SDS-PAGE and used to prepare three identical blots. The blots were overlaid with lysates from cells expressing wild-type CA4, CA4-R14W or CA4-R219S, and the amount of CA4 associated with NBC1 was determined by immunoblotting with anti-CA4 antibody, followed by quantitative analysis (Fig. 4C). The results show that CA4-R14W mutant bound to NBC1 3-fold less efficiently ( $34 \pm 5\%$ ,  $P < 0.05$ ), whereas interaction of inactive

CA4-R219S with NBC1 was similar to wild-type CA4. We conclude that biologically active CA4-R14W does not stimulate NBC1 activity by failing to bind to NBC1, whereas CA4-R219S does not stimulate NBC1 activity due to its enzymatic inactivity.

#### R14W mutant CA4 is not defective in secretion

Failure to activate NBC1 activity could also be explained if the CA4-R14W mutant was not secreted or incompetently anchored to the cell surface. To assess whether the CA4 mutants differed from wild-type CA4, we performed cell surface processing and secretion assays. In these experiments, CA4-expressing cells were exposed to the membrane-impermeant biotinylation reagent, EZ-Link<sup>TM</sup> Sulpho NHS SS Biotin. Biotinylated proteins (representing the protein present at the cell surface) will bind to streptavidin resin. The amount of biotinylated protein was assessed on immunoblots by measuring the total amount of CA4 present in the lysates, the amount that did not bind the streptavidin resin and the amount of CA4 that could be eluted from the resin. Figure 5A shows the amount of total, streptavidin resin-bound and eluted wild-type CA4, CA4-R14W and CA4-R219S. Quantification of the amount of biotinylated CA4 revealed that both mutants were processed to the cell surface to a degree indistinguishable from wild-type CA4 (Fig. 5B). These data show that only ~40% of each of the proteins was biotinylated and thus cell surface associated. This reflects the fact that a portion of each protein was retained in intracellular membranes during biosynthesis.

To further assess whether CA4-R14W mutant is defective in secretion, we generated fusion proteins where the N-terminal 18 amino acids, including the signal sequence of wild-type CA4 and CA4-R14W, replaced the signal sequence of the human alkaline phosphatase (AP) reporter gene (CA4WT-AP

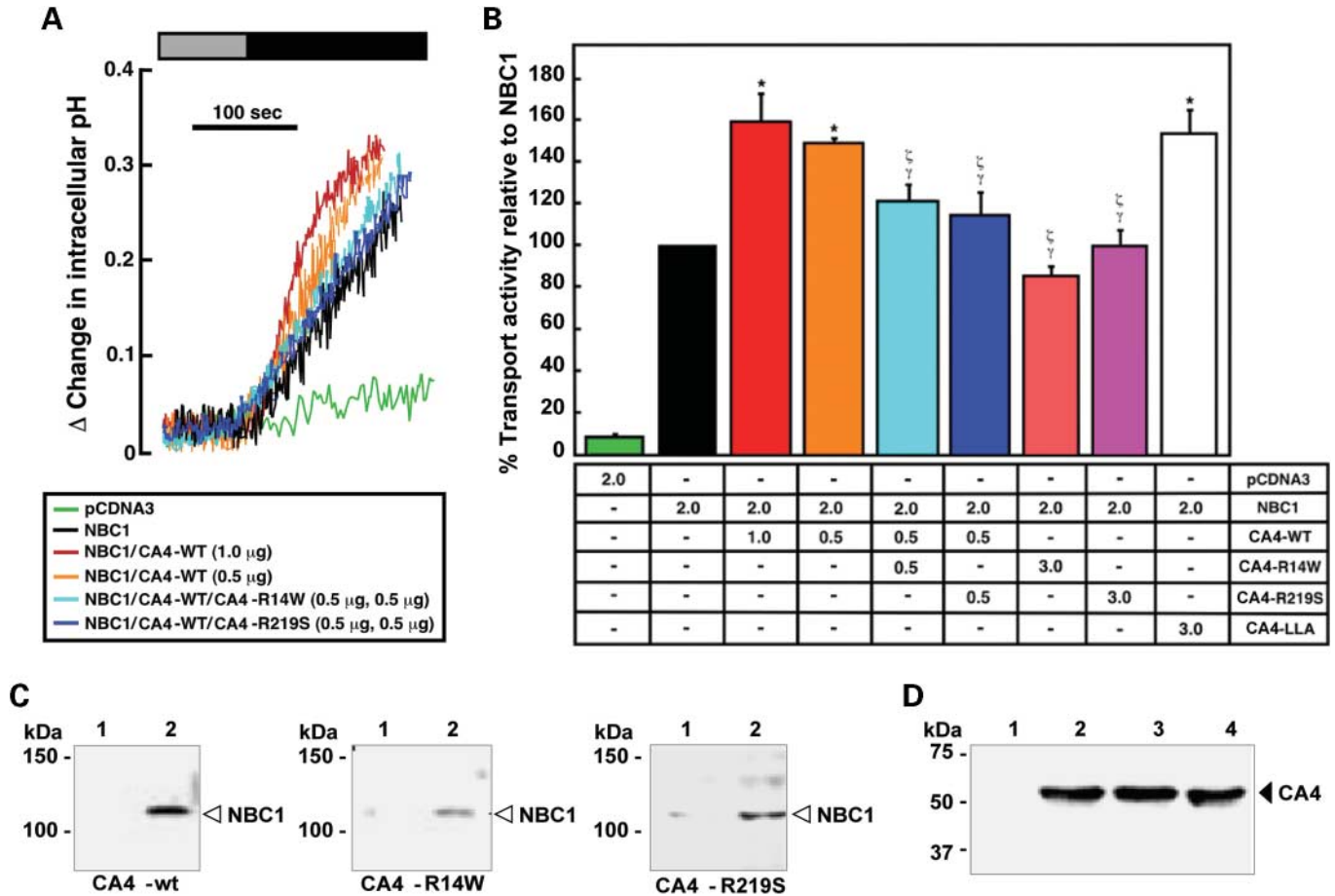


**Figure 4.** Effect of wild-type and mutant CA4 on NBC1 transport rate and binding. (A) Representative traces of pH<sub>i</sub> recovery in HEK293 cells transfected with empty vector (pcDNA3), NBC1, NBC1 and CA4-WT, NBC1 and CA4-WT, NBC1 and CA4-WT/CA4-R14W or NBC1 and CA4-WT/CA4-R219S (see inset legend). NBC1 cDNA (2 μg) was used, whereas CA4 cDNA is indicated in brackets. Acidification in NH<sub>4</sub>Cl (30 mM, gray bar) was followed by NBC1-mediated pH<sub>i</sub> recovery in bicarbonate-containing buffer (black bar). (B) Transport activity of cells transfected with cDNAs (microgram), indicated at the bottom. NBC1 flux was 4.78 ± 0.33 mm/min. For simplicity, NBC1 alone was set at 100%, all other data were expressed relative to this value. Bars with symbols <sup>\*</sup><sub>1-6</sub> indicate statistically significant difference (P < 0.05) compared with NBC1, NBC1/CA4-WT (1.0 μg) or NBC1/CA4-WT (0.5 μg), respectively. (C) Blot overlay assay of NBC1 with CA4-WT and mutants. Cell lysates (20 μg protein) from cells transfected with pcDNA3 (lane 1) or NBC1 cDNA (lane 2), were resolved by SDS-PAGE and transferred to PVDF membrane. Immunoblots were incubated with lysates prepared from cells expressing CA4-WT, CA4-R14W or CA4-R219S. CA4 associated with the NBC1 band (arrow) was detected with an anti-CA4 antibody. (D) Expression of CA4 in lysates used for overlays was measured on immunoblots probed with anti-human CA4 antibody: pcDNA3 (lane 1), CA4-WT (lane 2), CA4-R14W (lane 3) and CA4-R219S (lane 4).

and CA4R14W-AP, respectively). At the steady state level, the CA4R14W-AP was secreted comparable to CA4WT-AP (Fig. 5C). These data strongly suggest that both wild-type and R14W signal sequences are competent signal sequences to direct AP to the secretory pathway.

**DISCUSSION**

In this study, we show that two missense mutations in CA4 likely cause rod and cone photoreceptor degeneration by a novel pathogenic mechanism. Several lines of evidence support the contention that the missense changes CA4-R14W and CA4-R219S and perhaps a 3'-UTR + 59 A>G mutation in CA4 are pathogenic mutations. First, all changes segregated with the disease phenotype in families A, B and C (Fig. 1A), and neither change was present in over 1000

**Table 1.** CA4 enzymatic activity assay

Cell sample	SDS-resistant CA activity (μmol/min mg total protein)	Wild-type activity (%)
Vector-transfected cells	-19 ± 88	0
WT CA4	282 ± 41	100
R219S CA4	10 ± 39	4
R14W CA4	225 ± 41	80

The rate of carbon dioxide hydration was measured for lysates of HEK293 cells transfected with vector alone or with CA4 variants.

normal control chromosomes. Secondly, expression of either CA4-R14W or CA4-R219S mutant in the plasma membrane failed to increase the NBC1-mediated rates of pH<sub>i</sub> recovery after acid load (Fig. 4A and B). Therefore, we propose that the functional effect of CA4 on NBC1 activity is abolished

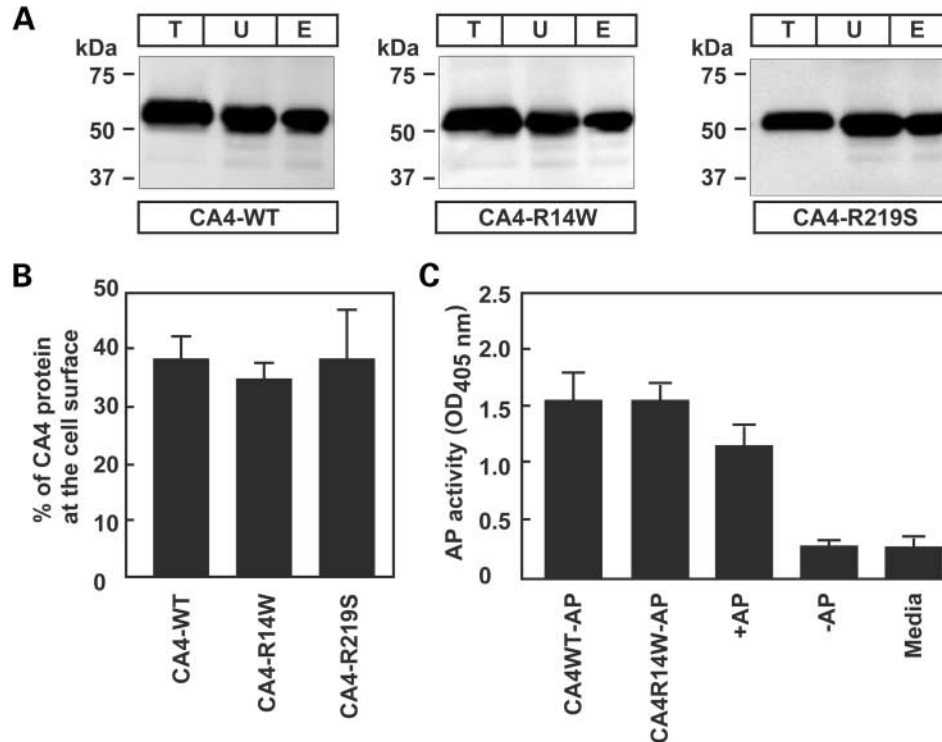


**Figure 5.** Cell-surface expression of CA4-WT and mutants. (A) HEK-293 cells, transfected with CA4-WT CA4-R14W or CA4-R219S cDNA, were incubated with the membrane-impermeant, lysine-directed compound, EZ-Link<sup>TM</sup> Sulpho-NHS-SS-Biotin. Cells were solubilized, and proteins were incubated with streptavidin resin. Biotinylated proteins associated with the resin were eluted with SDS-PAGE sample buffer. Protein samples [(T) total, (U) unbound and (E) eluted fractions] were electrophoresed on polyacrylamide gels and transblotted to PVDF membrane. Blots were developed using anti-CA4 antibody, incubated with ECL<sup>®</sup> reagent and imaged with a Kodak Image station. (B) Fraction of CA4 associated with the plasma membrane was quantified by densitometry of the immunoblotted proteins and calculated as [(Total - unbound)/total] × 100% ( $n = 3$ ). (C) Effect of R14W mutation on CA4 secretion. The ability of the CA4 N-terminal amino acid sequence, with the R14W mutation, to direct AP to the secretory pathway was measured for fusion proteins. The N-terminal 18 amino acid sequences of WT and R14W CA4 were fused to AP (CA4WT-AP and CA4R14W-AP respectively), +AP denoted AP with its native signal sequence as a positive control and -AP represented AP without a signal sequence as a negative control. Media only denoted transfection control where no DNA was added. Fusion protein secretion was measured as total amount of AP activity secreted into the media.

by these *CA4* mutations, either due to decreased physical interaction (R14W, Fig. 4C) or due to altered catalytic activity of CA4-R219S (Table 1). A disease causing mechanism of the 3'-UTR mutations has not been determined. In this context, it is worth noting that *NBC1* null mutations in human patients demonstrate an autosomal recessive inheritance pattern with proximal renal tubular acidosis, and severe ocular phenotypes including corneal opacities and glaucoma (23). Retinal dystrophy has not been reported in these patients, but cannot be ruled out as the patients are essentially blind and visualization of retina is difficult due to corneal opacities. Blindness and auditory impairment in mice have been reported recently due to null mutations in another NBC transporter (NBC3) (24). The failure of RP-causing mutants of CA4 to activate NBC1 may form the basis for RP in these patients. However, it is worth noting that CA4 also physically and functionally interacts with other pH-regulatory bicarbonate transporters of the SLC4A family ( $\text{Cl}^-/\text{HCO}_3^-$  exchangers) (25). As some of these  $\text{Cl}^-/\text{HCO}_3^-$  exchangers are also expressed in retina, a failure of CA4 mutants to activate retinal  $\text{Cl}^-/\text{HCO}_3^-$  exchange could also underlie the RP.

While our work was in progress, Rebello and co-workers (17) reported identification of the CA4-R14W mutation in different branches of the original RP17 family, confirming

further segregation of R14W with the disease phenotype. They also propose that R14W mutation causes impaired CA4 secretion, choroidal ischemia and subsequent apoptosis. However, our results indicated that both wild-type and mutant CA4 were secreted at an approximately comparable efficiency (Fig. 5) and present at the cell surface in a comparable amount (Fig. 5). In addition, patients with a CA4-R14W mutation do not have choroidal ischemia or atrophy as shown by fluorescein angiography and IndoCyanine Green angiography (K. Zhang, unpublished data). Therefore, we argue impaired pH regulation by the CA4/NBC1 complex, rather than a CA4 secretion defect, is the cause of photoreceptor degeneration phenotype.

In contrast to the expression pattern of all previously known genes causing RP (irrespective of the inheritance pattern), both CA4 and NBC1 are not expressed in photoreceptors or RPE at detectable levels, yet are highly expressed in choriocapillaris and other tissues. The lack of functional abnormalities in other tissues expressing CA4 (kidney, heart and lung) in RP17 patients suggests that one of several known CA isozymes may compensate for mutant CA4 in tissues other than eye. Alternatively, the limited tolerance of acidity of the visual system may cause the exclusive photoreceptor degeneration

phenotype. The extraordinarily high metabolic rate in photoreceptor cells and RPE requires that the choriocapillaris functions very effectively in maintaining pH homeostasis, and photoreceptor degeneration may result when pH homeostasis is impaired.

One of most widely used CA inhibitors, such as acetazolamide, is given frequently as an oral dosage of 500 mg twice daily. At this dosing regimen, it produces a serum trough and peak range of 12–30  $\mu\text{g/ml}$ , or 54–135  $\mu\text{M}$  in concentration (26). The  $\text{IC}_{50}$  of acetazolamide for CA4 is 4  $\mu\text{M}$  (27). The  $K_i$  of acetazolamide for CA4 is 70 nM (28), therefore current CA inhibitors will almost fully inhibit CA4 enzymatic activity comparable to a CA4 null mutation, and thus the use of these CA inhibitors may impair photoreceptor function. A study of healthy volunteers showed that a single dose of 500 mg of acetazolamide causes demonstrable changes in tests of color vision (29). In addition, light-adapted electroretinogram (ERG) a-waves are attenuated  $\sim 14\%$  by acetazolamide (30). Similar results have been reported in rats (31) and rabbits (32). Although acetazolamide may inhibit other potential CAs in the eye, these studies indicate a link of pH change and ERG. Therefore, we caution that long-term use of CA inhibitors may have potential detrimental effects on photoreceptor cells and vision.

## MATERIALS AND METHODS

### Subjects

Approval from the Institutional Review Board of the University of Utah, USA and Moorfields Eye Hospital, London, UK was obtained for this study, and informed consent was obtained from all patients. Twenty-two individuals at risk for inheriting RP in the first Caucasian kindred (family A), eight at risk for the disease in family B, three at risk for the disease in family C and one at risk for the disease in family D were participated in the study. All four families are of northern European origin, as are the 500 normal control subjects.

### Clinical investigations

A visual history was obtained from all patients, and best-corrected visual acuities were assessed. Ophthalmoscopic examination was performed on all patients, and fluorescein angiography on three affected patients. Reduction in night and peripheral vision appeared at around age 15, followed by progressive rod photoreceptor atrophy and bone spicule pigmentation (Fig. 1B). In addition, there is concomitant cone photoreceptor dysfunction manifested by photophobia, color vision changes and decreased central vision. Consistent with the notion that RP17 is a rod–cone dystrophy, ERG recordings demonstrated a reduction of both rod (scotopic) and cone (photopic and flicker) responses (Fig. 1C).

After initial dark adaptation, ERGs were recorded using a monopolar Burian-Allen contact lens electrode to strobe flash stimuli presented within an LKC ganzfeld using an established method (33). Reference and ground leads were placed on the forehead and earlobe, respectively. The response was

differentially amplified (band-pass: 0.3–500 Hz), averaged and stored using an LKC UTAS E-2000 signal-averaging system. Responses were initially recorded to flashes presented to the dark-adapted eye, using low intensity ( $-2.0 \log \text{cd s/m}^2$ ) and high intensity ( $0.5 \log \text{cd s/m}^2$ ) stimuli. A steady rod-desensitizing adapting field ( $1.5 \log \text{cd/m}^2$ ) was then presented in the ganzfeld bowl. After a 7 min period of light adaptation, cone ERGs were recorded to  $0.5 \log \text{cd s/m}^2$  flashes presented at 0.7 and 31 Hz.

### Genetic linkage and mutation screening

DNA was extracted from blood samples, and genetic linkage assessed using microsatellite markers D17S1290 and D17S948 tightly linked to the RP17 locus using established methods (34). An autosomal dominant mode of inheritance with full penetrance was used for LOD score computation. Disease allele frequency was set at 0.0001. Mutational screening of the eight exons of the *CA4* gene was performed by denaturing high-performance liquid chromatography (dHPLC) analysis followed by direct sequencing of PCR-amplified DNA fragments corresponding to each exon of the gene using established methods (35). PCR primers were designed on the basis of flanking intronic sequences of each exon according to published sequence (36). The complete coding region and the intron splice sites of the *CA4* gene were amplified by PCR. Amplified products were purified using the QIAquick Gel Extraction Kit (QIAGEN, Valencia, CA, USA) and sequenced with forward and reverse primers by the Taq Dyedexy Terminator Cycle Sequencing Kit (Beckman-Coulter, Fullerton, CA, USA) according to the manufacturer's instructions.

dHPLC (Transgenomics, Inc., Omaha, NE, USA) analysis was used to screen changes in *CA4* and to test the presence/absence of the mutation in the normal controls according to the manufacturer's instructions.

### Confocal immunolocalization of CA4 and NBC1

Eye tissues from a 12-year-old human donor were retrieved from the Lions Eye Bank of Utah, fixed using freshly prepared 4% paraformaldehyde in 0.1 M phosphate buffer (pH 7.4), cryoprotected using 30% sucrose in buffer and embedded in TBS<sup>TM</sup> tissue freezing medium (Triangle Biomedical Sciences, Durham, NC). Cryosections (12  $\mu\text{m}$  thick containing sclera, choroid, choriocapillaris, RPE and retina) were placed on gelatinized glass slides and stored at  $-70^\circ\text{C}$ .

For immunocytochemistry, sections were rinsed twice (5 min each) in phosphate-buffered saline (PBS) to remove the embedding medium and were incubated in 10% normal goat serum in PBS containing 0.1% Triton X-100 (PBS-T) for 1 h to block non-specific interactions. Rabbit affinity-purified anti-human lung CA4 polyclonal antibody (1:500, 40  $\mu\text{l}$ ) was applied to each eye section in a humidified, rotating chamber for 1–2 h at room temperature. The sections were rinsed thoroughly in three changes (10 min each) of fresh buffer before incubation for 1 h in affinity purified, fluorescein-conjugated goat anti-rabbit IgG (Jackson Immuno Research Laboratories). As in Figure 3A, propidium iodide (1:3000 dilution, Molecular Probes) was sometimes added

to the solution containing FITC-conjugated secondary antibody to provide contrast. The sections were rinsed thoroughly in PBS, blotted nearly dry, submerged under a drop of Vectashield (Vector Laboratories), coverslipped and viewed using a Zeiss LSM 510 inverted Laser Scan confocal microscope with a 40 $\times$  oil objective lens and optical slice setting of <1  $\mu$ m.

Sequential incubations were required to demonstrate colocalization of CA4 and NBC1 (Fig. 3D–F) as both polyclonal primary antibodies were raised in rabbits. Thus, after rinsing to remove embedding medium, the tissue sections were incubated for 1 h in 10% normal donkey serum in PBS-T. Affinity-purified anti-NBC1 antibody (raised against a C-terminal fragment of NBC1 protein in 1:1000, 50  $\mu$ l) was applied to each section in a humidified, rotating chamber overnight at 4°C. The sections were rinsed thoroughly in fresh buffer (10 min  $\times$  3) at room temperature prior to incubation for 1 h in affinity purified, rhodamine Red<sup>TM</sup>-X-conjugated donkey anti-rabbit IgG (Jackson Immuno Research Laboratories). The sections were rinsed again in fresh PBS (10 min  $\times$  3), and then incubated in 10% normal goat serum in PBS-T for 1 h. The anti-CA4 antibody (1:2000, 50  $\mu$ l) was applied for 1 h at room temperature. After rinsing extensively, FITC-conjugated goat anti-rabbit secondary antibody was applied for 1 h to visualize sites of CA4 immunoreactivity. The sections were rinsed again and viewed under the confocal microscope. Control incubations, consisting of omission of each primary antibody, were performed and imaged in parallel.

### Generation of expression constructs

The full-length wild-type and mutant *CA4* cDNAs were cloned separately into pcDNA3 vectors (Invitrogen, Carlsbad, CA, USA). This vector utilizes a CMV promoter driven expression following transfection into mammalian cells. PCR was performed using forward and reverse primers 5'-CGGGA TCCCGCGCAAGATGCGGATGCTGCTG-3' and 5'-ATAG TTTAGCGGCCGATTCTTATTCATCGCAGGAAGCCGGC CAG-3' (containing *Bam*HI and *Not*I restriction sites) using wild-type *CA4* cDNAs as templates. The resultant PCR products were digested with *Bam*HI and *Not*I, and cloned into the *Bam*HI and *Not*I sites of a pcDNA3 vector. The 40 C>T (R14W), 655 C>A (R219S) and 21\_29ins9 insertion (ins L<sub>7</sub>L<sub>8</sub>A<sub>9</sub>) were introduced into wild-type construct by PCR-based site-directed mutagenesis. The recombinant plasmids were purified using a Qiagen plasmid isolation kit (Qiagen Inc, Valencia, CA, and USA). NBC1 expression constructs have been described previously (15,37). All constructs were verified by restriction digest and DNA sequencing.

### Protein expression and cell surface processing assays

NBC1 (pNBC1 isoform expressed in the eye) and CA4 proteins were expressed by transient transfection of HEK293 cells (38,39), using the calcium phosphate method (40). Cells were grown at 37°C in an air/CO<sub>2</sub> (19:1) environment in DMEM medium, supplemented with 5% (v/v) fetal bovine serum and 5% (v/v) calf serum. Assays to assess the degree of cell surface processing and biotinylation of CA4 were performed as described previously (39).

### CA4-R14W secretion assay

For CA4 secretion assays, the first 54 coding nucleotides of CA4-WT and R14W mutant, encoding N-terminal 18 amino acids, were cloned into a modified version of APTag2 (41) and fused in frame with human AP at the C-terminal (yielding CA4WT-AP and CA4R14W-AP, respectively). PCR was performed using one forward primer 5'-ATAA GAATGCGGCCGCTAAACTATCTCGGTGCGCGACCCCG GC-3' and two reverse primers 5'-CCCAAGCTTGACTGG CCGATGGCCGCGC-3' and 5'-CCCAAGCTTGACTGGCC GATGGCCACGC-3' (containing *Not*I and *Hind*III restriction sites) using wild-type *CA4* cDNAs as templates. The resultant PCR products were digested with *Not*I and *Hind*III and cloned into the *Bam*HI and *Not*I sites of APTag2. CA4-AP fusion proteins (CA4WT-AP, CA4R14W-AP) were expressed by transient transfection of HEK293 cells. Secretion of these AP fusion proteins was monitored by measuring the enzymatic activity of AP in the culture media using an AP Assay Reagent A according to the manufacturer's instructions (GenHunter Corporation, Nashville, TN, USA). The dephosphorylation of the p-nitrophenyl phosphate by AP leads to the generation of a yellow color, which serves as a quantitative measurement of AP (absorbance at 405 nm).

### Co-expression of WT and mutant CA4

To assess the relationship between the amount of CA4 expression and NBC1 transport activity, HEK293 cells were co-transfected with a fixed amount (2  $\mu$ g) of *NBC1* cDNA and a varied amount (0–3  $\mu$ g) of *CA4* cDNA. Carrier DNA (pcDNA3 vector) was added so that DNA in each transfection totaled 5  $\mu$ g. Transport rates for NBC1 were measured for each of these samples. On the basis of these data, 1  $\mu$ g was found to be the minimum amount of *CA4* cDNA to maximize NBC1 activity (Supplementary Material, Fig. S2).

To examine the effect of CA4 mutants on NBC1 activity, NBC1 was co-expressed with wild-type and mutant *CA4* cDNAs. HEK293 cells were transfected with 2  $\mu$ g of *NBC1* cDNA and 0.5 or 1  $\mu$ g of *CA4* cDNA (0.5 or 1  $\mu$ g WT *CA4* or 0.5  $\mu$ g WT with 0.5  $\mu$ g *CA4*-R14W or *CA4*-R219S). Transport rates were assessed for the transfected cells as described subsequently.

Samples of the transfected cells were subjected to SDS-PAGE and transblotting. Expression of  $\beta$ -actin was detected with mouse monoclonal anti- $\beta$ -actin antibody (clone AC-74, Sigma) and CA4 was detected with rabbit polyclonal anti-human CA4 antibody. Expressions of  $\beta$ -actin and CA4 were quantified by densitometry. The expression level of  $\beta$ -actin, which indicated the amount of lysate assayed, was used to determine the amount of CA4 expressed in each cell. The normalized data indicated that total CA4 expression (WT plus mutant) was constant in each of the samples (Supplementary material Fig. S3).

### Immunodetection

HEK293 cells were transfected or co-transfected with pcDNA3 (empty vector), *NBC1*, *CA4*-WT and *CA4* mutant (*CA4*-R14W, *CA4*-R219S and *CA4*-LLA) cDNAs (19). Two days

post-transfection, cells were washed in PBS buffer (140 mM NaCl, 3 mM KCl, 6.5 mM Na<sub>2</sub>HPO<sub>4</sub>, 1.5 mM KH<sub>2</sub>PO<sub>4</sub>, pH 7.40) and lysates of the whole tissue culture cells were prepared by addition of 250  $\mu$ l SDS-PAGE sample buffer [20% (v/v) glycerol, 2% (v/v) 2-mercaptoethanol, 4% (w/v) SDS, 1% (w/v) bromophenol blue, 150 mM Tris, pH 6.8]. Samples (10  $\mu$ g protein) were resolved by SDS-PAGE on 10% acrylamide gels (42). Proteins were transferred to PVDF membranes, and then incubated with rabbit anti-rat NBC1 antibody, rabbit anti-human CA4 (19) or mouse anti-human  $\beta$ -actin monoclonal antibody. Immunoblots were incubated with donkey anti-rabbit IgG conjugated to horseradish peroxidase or sheep anti-mouse (Santa Cruz). Blots were visualized and quantified using ECL reagent and a Kodak Image Station by densitometry of the blots, which were co-developed for the same amount of time.

### Gel overlay assays

Gel overlay assays to detect NBC1 interactions with CA4-WT and CA4 mutants were performed as previously described (19,25). Briefly, HEK293 cells grown in 100 mm culture dishes were transiently transfected individually with cDNA encoding NBC1 or CA4-WT, or CA4 mutants, as described earlier. Two days post-transfection, cells expressing an NBC1 protein were solubilized in SDS-PAGE sample buffer and cells expressing CA4 were solubilized in 200  $\mu$ l IPB Buffer [1% (v/v) NP40, 5 mM EDTA, 150 mM NaCl, 0.5% (w/v) sodium deoxycholate, 10 mM Tris-HCl, pH 7.50], supplemented with protease inhibitors (Mini Complete tablets, Roche). Samples were sheared and centrifuged as described earlier. Immunoblots of lysates of cells transfected with NBC1 cDNA were prepared as described earlier. Immunoblots were blocked for 2 h with 10% TBST-M buffer [TBST buffer (0.1% v/v Tween-20, 137 mM NaCl, 20 mM Tris, pH 7.5) containing 5% w/v non-fat dry milk], then incubated overnight in 5% TBST-M containing 200  $\mu$ l of the cell lysate prepared from CA4 transfected cells. Immunoblots were then washed 3  $\times$  10 min in TBST and then probed for CA4 as described previously (19,25). We used lysates with an equal amount of CA4 by western blots using anti-CA4 antibody (Fig. 4D) or  $\beta$ -actin (data not shown).

### Assay of NBC1 activity

NBC1 activity was monitored using a fluorescence assay (19). Briefly, HEK293 cells grown on poly-L-lysine coated coverslips were transiently transfected. Two days post-transfection, coverslips were rinsed in serum-free DMEM and incubated in 4 ml serum-free media, containing 2  $\mu$ M BCECF-AM at 37°C for 20 min. Coverslips were mounted in a cuvette and perfused with Na<sup>+</sup>-free bicarbonate buffer solution (128.3 mM choline-Cl, 4.5 mM KCl, 1.35 mM CaCl<sub>2</sub>, 20.23 mM choline-HCO<sub>3</sub><sup>-</sup>, 1.05 mM MgSO<sub>4</sub>, 11 mM glucose, pH 7.40). NaCl and NaHCO<sub>3</sub> were replaced by equimolar amounts of choline-Cl and choline-HCO<sub>3</sub><sup>-</sup>, respectively, in the normal bicarbonate buffer solution. Both solutions were equilibrated with 5% CO<sub>2</sub>/air. HCO<sub>3</sub><sup>-</sup> transport activity of NBC1 ( $J_{\text{HCO}_3^-}$ ) was measured during the recovery from transient intracellular acidification. Cells were acid loaded by perfusion with

Na<sup>+</sup>-free bicarbonate buffer, containing 30 mM NH<sub>4</sub>Cl for 4–5 min, followed by the wash-out of NH<sub>4</sub>Cl with Na<sup>+</sup>-free bicarbonate buffer. After peak acidosis was reached, cells were perfused with Na<sup>+</sup>-free bicarbonate buffer for 2–3 min interval (plateau phase). The Na<sup>+</sup>-free bicarbonate buffer was then quickly replaced by normal bicarbonate buffer solution, and cells perfused for further 5–7 min (recovery phase). Assays were performed in the presence of 1 mM amiloride (Sigma) to block endogenous Na<sup>+</sup>/H<sup>+</sup> exchanger (NHE) activity. Fluorescence was monitored in a Photon Technologies International RCR fluorimeter, at excitation wavelengths 440 and 500 nm and emission wavelength 530 nm. Fluorescence ratios were converted to pH<sub>i</sub> by the nigericin/high potassium technique at three pH values between 6.5 and 7.5 (43). Initial rate of pH<sub>i</sub> recovery from an acid load was calculated by fitting a linear regression of either the first 1 min or 3 min of the pH<sub>i</sub> recovery (recovery phase) after maximum acidosis. In all cases, the transport activity of sham-transfected cells was subtracted from the total rate, to ensure that these rates consisted only of NBC1 transport activity.

To compare transport rates for NBC1 and NBC1/CA4 transfected cells, intrinsic buffer capacity ( $\beta_i$ ) was measured in HEK293 cells individually expressing NBC1 or expressing NBC1 and CA4 proteins.  $\beta_i$  values for HEK293 transfected with either NBC1 or NBC1 and CA4 were  $11.24 \pm 4.47$ , and  $15.32 \pm 4.26$ , respectively.  $\beta_i$  values estimated at similar pH<sub>i</sub> were  $6.82 \pm 0.10$  and  $6.80 \pm 0.10$  for either NBC1, or NBC1 and CA4, respectively. The total buffering capacity of the system ( $\beta_{\text{total}}$ ) was then determined as:  $\beta_{\text{total}} = \beta_i + \beta_{\text{CO}_2}$ , where  $\beta_{\text{CO}_2} = 2.3 \times [\text{HCO}_3^-]_i$ .  $\beta_{\text{total}}$  was  $26.93 \pm 4.49$  and  $30.30 \pm 4.39$  mM, for NBC1 and NBC1/CA4, respectively. We conclude that intrinsic and total buffering power did not differ in HEK293 expressing NBC1 alone or NBC1 and CA4 (data not shown).

The initial fall in pH<sub>i</sub> was similar in all eight groups, reaching an acid load peak of  $6.43 \pm 0.06$  (NBC1),  $6.42 \pm 0.06$  (NBC1/CA4-WT 0.5  $\mu$ g),  $6.39 \pm 0.07$  (NBC1/CA4-WT 1.0  $\mu$ g),  $6.38 \pm 0.02$  (NBC1/CA4-WT/CA4-R14W),  $6.33 \pm 0.05$  (NBC1/CA4-WT/CA4-R219S),  $6.43 \pm 0.03$  (NBC1/CA4-R14W),  $6.42 \pm 0.02$  (NBC1/CA4-R219S) and  $6.43 \pm 0.02$  (NBC1/CA4-LLA), ( $n = 4-8$ ; one-way ANOVA).

### Measurement of intrinsic buffer power and bicarbonate fluxes

Intracellular buffering power measurements were made by the ammonium pulse method (44). HEK293 cells grown on glass coverslips were transfected with NBC1 or co-transfected with NBC1 and CA4-WT cDNAs. Two days post-transfection, cells were loaded with BCECF-AM as described earlier. Coverslips were mounted in a fluorescence cuvette and allowed to equilibrate in HEPES-buffered solution, (140 mM NaCl, 11 mM glucose, 1.35 mM CaCl<sub>2</sub>, 1.05 mM MgSO<sub>4</sub>, 4.5 mM KCl, 20 mM Hepes), containing 1 mM amiloride, bubbled with 100% O<sub>2</sub> to ensure nominally bicarbonate-free conditions. Cells were then perfused consecutively for 300 s or until pH<sub>i</sub> was steady with HEPES-buffered solution, containing varying concentrations of NH<sub>4</sub>Cl (0, 1, 5, 10, 20 and 30 mM).  $[\text{NH}_4^+]_i$  was calculated from the Henderson-Hasselbach equation, and

the intrinsic buffer capacity ( $\beta_i$ ) was then calculated as  $\Delta[\text{NH}_4^+]_i/\Delta\text{pH}_i$ . The total buffering capacity of the system ( $\beta_{\text{total}}$ ) was then determined as:  $\beta_{\text{total}} = \beta_i + \beta_{\text{CO}_2}$ , where  $\beta_{\text{CO}_2} = 2.3 \times [\text{HCO}_3^-]_i$ . In transport assay, total flux of  $\text{HCO}_3^-$  equivalents was then calculated as:  $J_{\text{HCO}_3^-} = \beta_{\text{total}} \times \Delta\text{pH}_i/\Delta t$  (21).

#### CA4 activity assays

The assay procedure was a modified version of a protocol described previously (36,45). Transfected HEK293 cells were removed from 60 mm dishes by cell scraping. Cell pellets were resuspended in 500  $\mu\text{l}$  of 0.2% SDS in 5 mM Tris/ $\text{SO}_4$ , pH 7.9, containing protease inhibitors (Roche, mini-complete). Samples were incubated for 30–60 min at room temperature prior to assays. Unlike other CAs, CA4 is resistant to SDS denaturation, so that this assay reports only on CA4 enzymatic activity (36). All assay reagents were chilled in an ice bath prior to use. Each assay sample consisted of 6 ml of 1.67 mM Tris/ $\text{SO}_4$ , pH 7.9 and 100  $\mu\text{l}$  of sample. Assays were performed in glass test tubes in an ice-water bath, on a magnetic stir plate, which was stirred continuously. Recordings of pH as a function of time were initiated upon gassing the sample with 600 ml/min of carbon dioxide gas. CA activity was determined by linear regression of the rate of change of pH over the 7.8–7.5 range. The rate of change of pH in control samples (100  $\mu\text{l}$  of 0.2% SDS in 5 mM Tris/ $\text{H}_2\text{SO}_4$ , pH 7.9) was subtracted from each of the rates.

#### Real-time RT-PCR

To compare the relative expression level of *CA4* gene in patient with a 3'-UTR mutation and a normal individual, we performed quantitative real-time RT-PCR. The following primers were used for *CA4* PCR: forward 5'-ATACCAGGCCAAACAGTTGC-3' and reverse 5'-ATTCCTCGATGTCCCCTTCT-3'. The following primers were used for *GA PDH* PCR: forward 5'-GGAAGGTGAAGGTCGGAGTC-3' and reverse 5'-AATGAAGGGGTCATTGATGG-3'. Total RNA were isolated by using PURESRIPT RNA isolation kit (Gentra, Minneapolis, MN, USA) from peripheral lymphocytes of blood samples in affected and normal individuals. Real-time RT-PCR of *CA4* was performed in each sample using *GAPDH* as an internal control with the QuantiTect SYBER Green RT-PCR kit (Qiagen Inc, Valencia, CA, USA). Real-time PCR was performed on a DNA Engine Opticon 2 system (MJ Research, Waltham, MA, USA). Amplification efficiency of *CA4* was determined relative to *GAPDH* as an internal control according to the manufacturer's instructions (Supplementary Material, Fig. S1). Amount of *CA4* in each sample was calculated by a comparative or  $\Delta\Delta$  Ct (threshold cycle) value method according to the manufacturer's instructions (Qiagen Inc, Valencia, CA, USA).

#### Statistical analysis

Statistical significance in transfection studies was evaluated using paired *t*-test, or one way-ANOVA, as indicated, with  $P < 0.05$  considered significant. Error bars show standard error of the mean ( $n = 3-5$ ).

## SUPPLEMENTARY MATERIAL

Supplementary Material is available at HMG Online.

## ACKNOWLEDGEMENTS

We dedicate this article to Mr Nick Malherbe who passed away recently, whose tireless effort and support made the success of this project possible. We are grateful to patients and their families for participation in this study. We thank Dr Antoine Bril (GlaxoSmithKline, USA) for *NBC1* cDNA, Dr Manoocher Soleimani for affinity purified anti-NBC1 antibody and Dr William Sly for anti-CA4 antibody. We thank Kim Howes, Guy Zimmerman, Jeremy Nathans and Nicholas Katsanis for advice and critical reading of the manuscript. We thank Drs Samuel Jacobson, Stephen Daiger, Sara Browne, Lori Sullivan, Carmel Toomes, Chris Inglehearn, Yang Li and Paul Bernstein for sharing DNA samples and DNA testing. J.R.C. is a Senior Scholar of AHFMR. This research is supported by grants from the NIH (RO1EY14428, RO1EY14448, EY08123, GCRC M01-RR00064); The Ruth and Milton Steinbach Fund; Ronald McDonald House Charities; the Macular Vision Research Foundation; the Research to Prevent Blindness, Inc.; Canadian Institutes of Health Research; Center Grants from Foundation Fighting Blindness, Inc.; and the British Retinitis Pigmentosa Society.

## REFERENCES

- Humphries, P., Kenna, P. and Farrar, G.J. (1992) On the molecular genetics of retinitis pigmentosa. *Science*, **256**, 804–808.
- Rivolta, C., Sharon, D., DeAngelis, M.M. and Dryja, T.P. (2002) Retinitis pigmentosa and allied diseases: numerous diseases, genes, and inheritance patterns. *Hum. Mol. Genet.*, **11**, 1219–1227.
- Pacione, L.R., Szego, M.J., Ikeda, S., Nishina, P.M. and McInnes, R.R. (2003) Progress toward understanding the genetic and biochemical mechanisms of inherited photoreceptor degenerations. *Annu. Rev. Neurosci.*, **26**, 657–700.
- Rattner, A., Sun, H. and Nathans, J. (1999) Molecular genetics of human retinal disease. *Annu. Rev. Genet.*, **33**, 89–131.
- Donner, K., Hemilä, S., Kalamkarov, G., Koskelainen, A., Pogozeva, I. and Rebrik, T. (1990) Sulfhydryl binding reagents increase the conductivity of the light-sensitive channel and inhibit phototransduction in retinal rods. *Exp. Eye Res.*, **51**, 97–105.
- Liebman, P.A., Mueller, P. and Pugh, E.N., Jr (1984) Protons suppress the dark current of frog retinal rods. *J. Physiol. (Lond.)*, **347**, 85–110.
- Gedney, C. and Ostroy, S.E. (1978) Hydrogen ion effects of the vertebrate photoreceptor. The pK's of ionizable groups affecting cell permeability. *Arch. Biochem. Biophys.*, **188**, 105–113.
- Wangsa-Wirawan, N.D. and Linsenmeier, R.A. (2003) Retinal oxygen: fundamental and clinical aspects. *Arch. Ophthalmol.*, **121**, 547–557.
- Winkler, B.S. (1986) Buffer dependence of retinal glycolysis and ERG potentials. *Exp. Eye Res.*, **42**, 585–593.
- Meyerothen, E.P., Wilson, M.J. and Ostroy, S.E. (1986) The effects of HEPES, bicarbonate and calcium on the cGMP content of vertebrate rod photoreceptors and the isolated electrophysiological effects of cGMP and calcium. *Vision Res.*, **26**, 521–533.
- Krizaj, D. and Copenhagen, D.R. (1998) Compartmentalization of calcium extrusion mechanisms in the outer and inner segments of photoreceptors. *Neuron*, **21**, 249–256.
- Boron, W.F. and Boulpaep, E.L. (1989) The electrogenic  $\text{Na}/\text{HCO}_3$  cotransporter. *Kidney Int.*, **36**, 392–402.
- Soleimani, M. and Burnham, C.E. (2001)  $\text{Na}^+/\text{HCO}_3^-$  cotransporters (NBC): cloning and characterization. *J. Membr. Biol.*, **183**, 71–84.
- Soleimani, M., Grassi, S.M. and Aronson, P.S. (1987) Stoichiometry of  $\text{Na}^+/\text{HCO}_3^-$  cotransport in basolateral membrane vesicles isolated from rabbit renal cortex. *J. Clin. Invest.*, **79**, 1276–1280.

15. Choi, I., Romero, M.F., Khandoudi, N., Bril, A. and Boron, W.F. (1999) Cloning and characterization of a human electrogenic  $\text{Na}^+/\text{HCO}_3^-$  cotransporter isoform (hhNBC). *Am. J. Physiol.*, **276**, C576–C584.
16. Srere, P.A. (1987) Complexes of sequential metabolic enzymes. *Annu. Rev. Biochem.*, **56**, 89–124.
17. Rebello, G., Ramesar, R., Vorster, A., Roberts, L., Ehrenreich, L., Oppon, E., Gama, D., Bardien, S., Greenberg, J., Bonapace, G. *et al.* (2004) Apoptosis-inducing signal sequence mutation in carbonic anhydrase IV identified in patients with the RP17 form of retinitis pigmentosa. *Proc. Natl Acad. Sci. USA*, **101**, 6617–6622.
18. Bardien, S., Ebenezer, N., Greenberg, J., Inglehearn, C.F., Bartmann, L., Goliath, R., Beighton, P., Ramesar, R. and Bhattacharya, S.S. (1995) An eighth locus for autosomal dominant retinitis pigmentosa is linked to chromosome 17q. *Hum. Mol. Genet.*, **4**, 1459–1462.
19. Alvarez, B.V., Loiselle, F.B., Supuran, C.T., Schwartz, G.J. and Casey, J.R. (2003) Direct extracellular interaction between carbonic anhydrase IV and the human NBC1 sodium/bicarbonate co-transporter. *Biochemistry*, **42**, 12321–12329.
20. Hageman, G.S., Zhu, X.L., Waheed, A. and Sly, W.S. (1991) Localization of carbonic anhydrase IV in a specific capillary bed of the human eye. *Proc. Natl Acad. Sci. USA*, **88**, 2716–2720.
21. Roos, A. and Boron, W.F. (1981) Intracellular pH. *Physiol. Rev.*, **61**, 296–434.
22. Stams, T., Nair, S.K., Okuyama, T., Waheed, A., Sly, W.S. and Christianson, D.W. (1996) Crystal structure of the secretory form of membrane-associated human carbonic anhydrase IV at 2.8—*a resolution*. *Proc. Natl Acad. Sci. USA*, **93**, 13589–13594.
23. Igarashi, T., Inatomi, J., Sekine, T., Cha, S.H., Kanai, Y., Kunimi, M., Tsukamoto, K., Satoh, H., Shimadzu, M., Tozawa, F. *et al.* (1999) Mutations in SLC4A4 cause permanent isolated proximal renal tubular acidosis with ocular abnormalities. *Nat. Genet.*, **23**, 264–266.
24. Bok, D., Galbraith, G., Lopez, I., Woodruff, M., Nusinowitz, S., Beltrandel Rio, H., Huang, W., Zhao, S., Geske, R., Montgomery, C. *et al.* (2003) Blindness and auditory impairment caused by loss of the sodium bicarbonate cotransporter NBC3. *Nat. Genet.*, **34**, 313–319.
25. Sterling, D., Alvarez, B.V. and Casey, J.R. (2002) The extracellular component of a transport metabolon. Extracellular loop 4 of the human AE1  $\text{Cl}^-/\text{HCO}_3^-$  exchanger binds carbonic anhydrase IV. *J. Biol. Chem.*, **277**, 25239–25246.
26. Friedland, B.R., Mallonee, J. and Anderson, D.R. (1977) Short-term dose–response characteristics of acetazolamide in man. *Arch. Ophthalmol.*, **95**, 1809–1812.
27. Ives, H.E. (1998) In Katzung, B.G. (ed.), *Basic and Clinical Pharmacology*. Appleton and Lange, Stamford, CT, pp. 246–248.
28. Ilies, M.A., Vullo, D., Pastorek, J., Scozzafava, A., Ilies, M., Caproiu, M.T., Pastorekova, S. and Supuran, C.T. (2003) Carbonic anhydrase inhibitors. Inhibition of tumor-associated isozyme IX by halogenosulfanilamide and halogenophenylaminobenzolamide derivatives. *J. Med. Chem.*, **46**, 2187–2196.
29. Leys, M.J., van, S.S., Nork, T.M. and Odom, J.V. (1996) Acetazolamide affects performance on the Nagel II anomaloscope. *Graefes Arch. Clin. Exp. Ophthalmol.*, **234** (Suppl. 1), S193–S197.
30. Odom, J.V., Nork, T.M., Schroeder, B.M., Cavender, S.A., van, S.S. and Leys, M. (1994) The effects of acetazolamide in albino rabbits, pigmented rabbits, and humans. *Vision Res.*, **34**, 829–837.
31. Findl, O., Hansen, R.M. and Fulton, A.B. (1995) The effects of acetazolamide on the electroretinographic responses in rats. *Invest. Ophthalmol. Vision Sci.*, **36**, 1019–1026.
32. Broeders, G.C., Parmer, R. and Dawson, W.W. (1988) Electroretinal changes in the presence of a carbonic anhydrase inhibitor. *Ophthalmologica*, **196**, 103–110.
33. Peachey, N.S., Alexander, K.R. and Fishman, G.A. (1989) The luminance-response function of the dark-adapted human electroretinogram. *Vision Res.*, **29**, 263–270.
34. Kniazeva, M., Chiang, M.F., Morgan, B., Anduze, A.L., Zack, D.J., Han, M. and Zhang, K. (1999) A new locus for autosomal dominant stargardt-like disease maps to chromosome 4. *Am. J. Hum. Genet.*, **64**, 1394–1399.
35. Zhang, K., Kniazeva, M., Han, M., Li, W., Yu, Z., Yang, Z., Li, Y., Metzker, M.L., Allikmets, R., Zack, D.J. *et al.* (2001) A 5-bp deletion in ELOVL4 is associated with two related forms of autosomal dominant macular dystrophy. *Nat. Genet.*, **27**, 89–93.
36. Okuyama, T., Sato, S., Zhu, X.L., Waheed, A. and Sly, W.S. (1992) Human carbonic anhydrase IV: cDNA cloning, sequence comparison, and expression in COS cell membranes. *Proc. Natl Acad. Sci. USA*, **89**, 1315–1319.
37. Romero, M.F., Hediger, M.A., Boulpaep, E.L. and Boron, W.F. (1997) Expression cloning and characterization of a renal electrogenic  $\text{Na}^+/\text{HCO}_3^-$  cotransporter. *Nature*, **387**, 409–413.
38. Khandoudi, N., Albadine, J., Robert, P., Krief, S., Berrebi-Bertrand, I., Martin, X., Bevenssee, M.O., Boron, W.F. and Bril, A. (2001) Inhibition of the cardiac electrogenic sodium bicarbonate cotransporter reduces ischemic injury. *Cardiovasc. Res.*, **52**, 387–396.
39. Sterling, D., Reithmeier, R.A. and Casey, J.R. (2001) Carbonic anhydrase: in the driver's seat for bicarbonate transport. *J. Pancreas*, **2**, 165–170.
40. Ruetz, S., Lindsey, A.E., Ward, C.L. and Kopito, R.R. (1993) Functional activation of plasma membrane anion exchangers occurs in a pre-Golgi compartment. *J. Cell Biol.*, **121**, 37–48.
41. Flanagan, J.G. and Cheng, H.J. (2000) Alkaline phosphatase fusion proteins for molecular characterization and cloning of receptors and their ligands. *Methods Enzymol.*, **327**, 198–210.
42. Laemmli, U.K. (1970) Cleavage of structural proteins during the assembly of the head of bacteriophage T4. *Nature*, **227**, 680–685.
43. Thomas, J.A., Buchsbaum, R.N., Zimniak, A. and Racker, E. (1979) Intracellular pH measurements in Ehrlich ascites tumor cells utilizing spectroscopic probes generated *in situ*. *Biochemistry*, **18**, 2210–2218.
44. Boron, W.F. and De, W.P. (1976) Intracellular pH transients in squid giant axons caused by  $\text{CO}_2$ ,  $\text{NH}_3$ , and metabolic inhibitors. *J. Gen. Physiol.*, **67**, 91–112.
45. Sato, S., Zhu, X.L. and Sly, W.S. (1990) Carbonic anhydrase isozymes IV and II in urinary membranes from carbonic anhydrase II-deficient patients. *Proc. Natl Acad. Sci. USA*, **87**, 6073–6076.